Tl–Pt(CN)$_5$ in the Solid State—A Multimethod Study of an Unusual Compound Containing Inorganic Wires**

Farideh Jalilehvand,[a] Lars Eriksson,[b] Julius Glaser,*[a] Mikhail Maliarik,[a, e] János Mink,[a, c] Magnus Sandström,*[b] Imre Tóth,[a, f] and Józef Tóth[d]

Abstract: The crystal and molecular structure of a polycrystalline powder with a metal–metal bond and the composition TlPt(CN)$_5$ has been determined by combining results from X-ray powder diffraction (XRD), extended X-ray absorption fine structure (EXAFS) and vibrational spectroscopic studies. The XRD data gave the tetragonal space group *P*4/*nmm* (No. 129), with $a =$ 7.647(3), $c = 8.049(3)$ Å, $Z = 2$, and well-determined positions of the heavy metal atoms. The Pt–Tl bond length in the compound is 2.627(2) Å. The platinum atom coordinates four equivalent equatorial cyano ligands, with a fifth axial CN ligand and a thallium atom completing a distorted octahedral coordination geometry. The Tl–Pt(CN)$_5$ entities are linked together in linear –NC-Pt-Tl-NC-Pt-Tl chains through the axial cyano ligand. These linear "wires" are the essential structural features and influence the properties of the compound. A three-dimensional network is formed by the four equatorial cyano ligands of the platinum atom that form bridges to the thallium atoms of neighbouring antiparallel chains. The platinum atom and the five nitrogen atoms from the bridging cyano groups form a distorted octahedron around the thallium atom. EXAFS data were recorded at the Pt and Tl L_{III} edges for a more complete description of the local structure around the Pt and Tl atoms. The excessive multiple scattering was evaluated by means of the FEFF program. Raman and infrared absorption spectroscopy reveal strong coupling of the vibrational modes of the TlPt(CN)$_5$ entities, in particular the metal–metal stretching mode, which is split into four Raman and two IR bands. Factor group theory shows that a structural unit larger than the crystallographic unit cell must be used to assign vibrational bands. Intra- and intermolecular force constants have also been calculated. The compound exhibits red luminescence at 700 ± 3 nm in glycerol and has a corresponding excitation maximum at 240 nm. X-ray photoelectron spectra (XPS) show that the metal atoms have intermediate oxidation states, $Pt^{3.2+}$ and $Tl^{1.6+}$, between those in the parent Pt^{II} and Tl^{III} species and the decomposition products, Pt^{IV} and Tl^{I}. The solid compound TlPt(CN)$_5$ is stable to 520 °C. However in presence of water, a two-electron transfer between the metal atoms results in the cleavage of the metal–metal bond at 80 °C, forming a Pt^{IV} pentacyanohydrate complex and a monovalent thallium ion.

Keywords: cyanides · EXAFS spectroscopy · platinum · thallium · X-ray diffraction

[a] Prof. Dr. J. Glaser, Dr. F. Jalilehvand, Tekn. Lic. M. Maliarik, Prof. Dr. J. Mink, Ass. Prof. Dr. I. Tóth
Department of Chemistry, Inorganic Chemistry
The Royal Institute of Technology (KTH)
10044 Stockholm (Sweden)
Fax: (+46) 8-212626
E-mail: julius@inorg.kth.se

[b] Prof. Dr. M. Sandström, Ass. Prof. Dr. L. Eriksson
Division of Structural Chemistry, Arrhenius Laboratory
Stockholm University, 10691 Stockholm (Sweden)
Fax: (+46) 8-163118
E-mail: magnuss@struc.su.se

[c] Prof. Dr. J. Mink
Institute of Isotopes and Surface Chemistry
Chemical Research Center of the Hungarian Academy of Sciences
P.O. Box 77, 1525 Budapest (Hungary)
and Analytical Chemistry Department, University of Veszprém
P.O. Box 158, 8201 Veszprém (Hungary)

[d] Dr. J. Tóth
Institute of Nuclear Research
Hungarian Academy of Sciences (ATOMKI)
4001 Debrecen, P.O. Box 51 (Hungary)

[e] Tekn. Lic. M. Maliarik
Permanent address:
Kurnakov Institute of General and Inorganic Chemistry
Russian Academy of Sciences, Leninsky Prospect 31
Moscow 117907 (Russia)

[f] Ass. Prof. Dr. I. Tóth
Permanent address:
Department of Inorganic and Analytical Chemistry
Debrecen University (KLTE), 4010 Debrecen, Pf. 21 (Hungary)

[**] New Classes of Oligonuclear Platinum-Thallium Compounds with a Direct Metal–Metal Bond, Part 4. For Part 3 see ref. [6].

Supporting information for this article is available on the WWW under http://www.wiley-vch.de/home/chemistry/ or from the author. Fractional atomic position parameters for TlPt(CN)$_5$, as obtained from the powder diffraction data in the space group *P*4/nmm (No. 129); results of analyses of Pt L_{III} and Tl L_{III} edge EXAFS data; bond lengths and angles compared with the corresponding combined XRD/EXAFS results. Figures showing: Pt L_{III} EXAFS filtered functions for the solid $K_2[Pt^{II}(CN)_4] \cdot 3H_2O$, together with the model fits and corresponding Fourier transforms; description of internal coordinates in the model including eight axial formula units ($Z = 8$), used for force constant calculations.

  0947-6539/01/0710-2167 $ 17.50+.50/0

Introduction

Recently, heteronuclear cyanide-bridged complexes of transition metals have attracted much attention because of their unusual photoredox reactions.[1] A light-induced metal-to-metal charge-transfer (MMCT) transition is mediated through the linear M-CN-M′ bridge between the two different metal atoms, which are in their oxidised and reduced forms. This leads to changes in the oxidation states of the metal ions and, in particular situations, can result in reversible dissociation of the compound. Applications of such inorganic systems in the fields of photocatalysis, solar energy conversion and artificial photosynthesis are foreseen. The mechanism of the electron-transfer process, which can involve more than one electron, is also interesting from a theoretical point of view.

Only di- and trinuclear complexes of this class of compounds have been fully characterised[2] although polymeric $[-\text{M-CN-M}'-]_n$ chains can be prepared by electrochemical techniques.[3] However, linear arrangements of M-CN-M′ entities are also known in a number of one-dimensional polymers,[4] in which the oxidation states do not permit electron transfer between adjacent metal centres.

On the other hand, several heteronuclear transition metal complexes with a direct, unsupported and polar metal–metal M–M′ bond have been shown to undergo photoinduced MMCT redox reactions.[5] As far as we know, no oligometallic compound has been described that comprises of both types of electronic metal–metal links, that is, a nonbuttressed direct M–M′ bond and a linear M-CN-M′ bridge. A combination of both short and long interactions between heterometal centres in mixed-valence compounds may allow, in principle, two different types of MMCT reactions and could lead to new and interesting properties.

In this paper we describe a heterometallic cyano compound with an unusual linear-chain structure of alternating M–M′ and M-CN-M′ entities. The metal atoms are platinum and thallium, which are formally in their di- and trivalent oxidation states, respectively; this makes a two-electron charge transfer possible. This study is related to our previous investigations of a family of oligometallic platinum-thallium cyano complexes, which consist of the $[(NC)_5Pt-Tl(CN)_n]^{n-}$ ($n=0-3$) dimers and the $[(NC)_5Pt-Tl-Pt(CN)_5]^{3-}$ trimer with a direct and unsupported metal–metal bond.[6] The oligometallic species are formed in aqueous solution by reactions between the $[Pt^{II}(CN)_4]^{2-}$ and $[Tl^{III}(CN)_n]^{3-n}$ ($n=1-4$) cyano complexes, and can be regarded as metastable intermediates in a net two-electron transfer from the platinum(II) to the thallium(III) atom.

A white powder of the composition $TlPt(CN)_5$ precipitates from aqueous solutions that contain oligometallic Pt–Tl species under certain conditions.[6b] All attempts to obtain single crystals failed, so a study of the structure and bonding of this compound was performed by combining results from X-ray powder diffraction (XRD), EXAFS at the Pt and Tl L_{III} absorption edges, and vibrational (Raman and IR) spectroscopy. Some chemical properties and photophysical characteristics (absorption, emission, and X-ray photoelectron, XPS) of the $TlPt(CN)_5$ compound are also reported.

Results and Discussion

Formation and characterisation of the solid $TlPt(CN)_5$ compound: The equilibrium between the bimetallic species $[(NC)_5Pt-Tl(CN)_n]^{n-}$ in aqueous solution at high acidity and/or low free-cyanide concentration is shifted toward the uncharged complex $[(NC)_5Pt-Tl(H_2O)_x]$.[6d] Slow precipitation of a white powder occurs from such solutions. Elemental analysis shows that this compound contains platinum, thallium and cyanide in the molar ratio 1:1:5. This is consistent with results from XPS measurements. Lines characteristic for the elements Pt, Tl, C and N were obtained in the photoelectron spectrum of the solid sample. Neither of these analytical methods indicate the presence of water in the compound.

The solid is sparingly soluble ($< \approx 3.7$ mm) in slightly acidic aqueous solution. The ^{205}Tl NMR spectrum of such a solution shows a pseudo triplet with an intensity ratio of ≈1:4:1. This pattern is characteristic of binuclear Pt–Tl complexes and arises from spin–spin coupling between the ^{205}Tl and ^{195}Pt nuclei (^{195}Pt: $I=1/2$, natural abundance 33.8%).[6b] Both the chemical shift and the coupling constant are strongly pH-dependent ($\delta_{Tl}=900$, $^1J(^{195}Pt,^{205}Tl)=66$ kHz at pH = 5; $\delta_{Tl}\approx 780$, $^1J(^{195}Pt,^{205}Tl)=71$ kHz at lower pH) and agree with the corresponding values of the complex $[(NC)_5Pt-Tl(H_2O)_x]$, which was characterised previously in aqueous solution.[6b] The apparent pH-dependence can be attributed to the deprotonation of water molecules in the thallium coordination sphere; this occurs at low acid concentration. The hydrolysed and protonated species are in fast exchange on the Tl NMR timescale in aqueous solution; this prevents their separate detection. In aqueous solutions of ionic cyanides, the formation of $[(NC)_5Pt-Tl(CN)_n]^{n-}$ ($n=1-3$) species leads to higher solubility of the solid compound.[6b,d] Thus the formation conditions, the dissolution products and the stoichiometric composition, $TlPt(CN)_5$, of the solid powder strongly indicate that its structure is closely related to that of the neutral hydrated complex $[(NC)_5Pt-Tl(H_2O)_x]$, which is formed in aqueous solution.

Structure of the $TlPt(CN)_5$ compound: X-ray powder diffraction data were collected (Figure 1) and the crystal structure

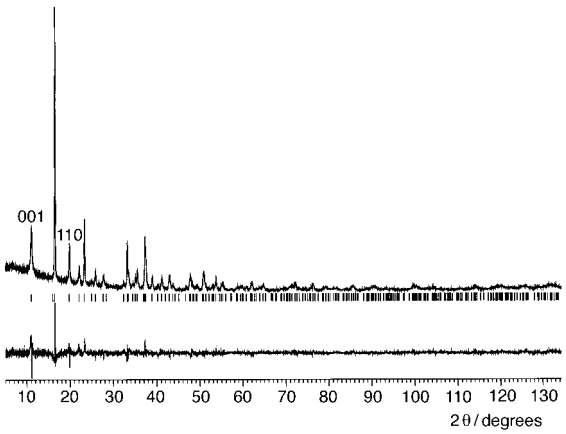

Figure 1. X-ray powder diffraction intensity of $TlPt(CN)_5$ as a function of the scattering angle 2Θ Upper trace: experimental intensity data, I_{obs}. Lower trace: $I_{obs}-I_{calc}$. The vertical markers show calculated peak positions.

0947-6539/01/0710-2168 $ 17.50+.50/0 *Chem. Eur. J.* **2001**, *7*, No. 10

was solved and refined by Rietveld methods (see the Experimental Section and Table 1 for details). The XRD positional parameters showed that the heavy metal atoms and an "axial" cyano group (C2–N2) are positioned on a four-fold axis and form linear –N2-C2-Pt-Tl-N2-C2-Pt-Tl– chains along the *c* axis of the unit cell (Figure 2 top). The space-group symmetry *P*4/*nmm* requires the four "equatorial" cyano ligands (C1–N1) of the platinum atom to be crystallographically equivalent. The nitrogen atoms (N1) of these equatorial cyano groups bridge the thallium atoms from the neighbouring antiparallel chains, and the nitrogen atom (N2) of the axial cyano ligand forms a short linear bond to the thallium atom within the chain. The atomic positional parameters obtained from X-ray powder diffraction (XRD) gave a precise value of the Pt–Tl seperation, but improbable values for the bond lengths that involve some of the lighter atoms. For example, the Pt–C1 bond length appeared as 1.80(2) Å (see Supporting Information) although Pt–C separations in cyano complexes of both platinum(II) and platinum(IV) fall in the range 1.97–2.01 Å.[7] Moreover, the C1–N1 bond length for a cyano ligand appeared much longer (≈1.5 Å) than that expected (≈1.15 Å).[8] The bond length obtained for the axial cyano ligand C2–N2 was not precise at 1.10(5) Å (see Supporting Information), but was within the range of expectation.

Thus the XRD data, which is dominated by scattering from the heavy atoms Pt and Tl, indicates disorder of the equatorial cyano groups. EXAFS measurements were performed to improve the description of the local structure around the metal atoms. The unit-cell dimensions and heavy atom positions from the XRD method were used as the basis of the description of the crystal structure and the Pt L_{III} and Tl L_{III} EXAFS data provide structural information on the coordination of the light atoms (Figure 3). The initial XRD positions of the disordered atoms C1 and N1 (given in the Supporting Information) were adjusted until a description of the structure was achieved (Tables 2 and 3) that was consistent with the EXAFS results. The consistency of the results is illustrated by the good agreement between the values of the Pt–Tl bond length, which can be obtained independently from both the Pt L_{III} and Tl L_{III} EXAFS (2.627 Å, Supporting Information) and from the XRD data (2.628 Å, Table 2).

Table 1. X-ray data collection parameters, crystal data and refinement indicators for the crystalline powder $TlPt(CN)_5$.[a]

Radiation	$Cu_{K\alpha 1}$ ($\lambda \approx 1.5406$ Å)
2Θ-range and step [°]	10.00–0134.98, $\Delta\Theta = 0.02$
number of reflections	278
total no. of parameters in Rietveld refinement	20
a [Å]	7.647(3)
c [Å]	8.049(3)
V [Å^3]	470.7(4)
Z	2
space group	*P*4/*nmm* (No. 129)
ρ_{calcd} [g cm^{-3}]	3.74
F(000)	448
$\mu(Cu_{K\alpha 1})$ [cm^{-1}]	595
halfwidth parameter, *U*	0.88(3)
halfwidth parameter, *V*	–0.14(2)
halfwidth parameter, *W*	0.027(2)
$RP = \Sigma \mid y_{oi} - y_{ci} \mid / \Sigma \mid y_{ci} \mid$	0.084
$R_wP = (\Sigma w_i (y_{oi} - y_{ci})^2 / \Sigma w_i \cdot y_{oi}^2)^{1/2}$	0.111
$R - I = \Sigma \mid I_o - I_c \mid / \Sigma \mid I_i \mid$	0.099
$R - F = \Sigma \mid \mid F_o \mid - \mid F_c \mid \mid / \Sigma \mid F_o \mid$	0.053
S (GooF)	1.2
DW	0.31

[a] For the abbreviations, see ref. [33].

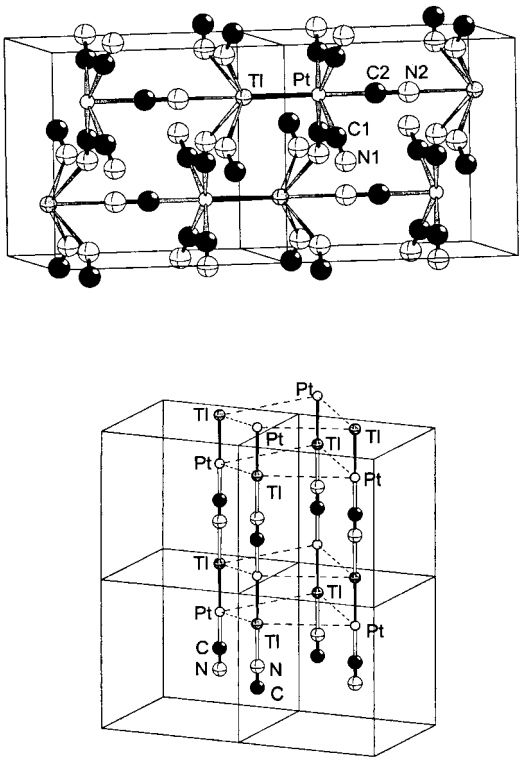

Figure 2. Structure of the compound $TlPt(CN)_5$. Top: Two unit cells showing the linear antiparallel –N2-C2-Pt-Tl-N2-C2-Pt-Tl– chains along the *c* axis (distances in Å). Bottom: Enlarged unit cell for the analysis of the Pt–Tl stretching vibrations.

Table 2. Bond lengths and angles for the solid sample $TlPt(CN)_5$, calculated using the parameters in Table 3. The accuracy of the distances involving light atoms is estimated to approximately 0.02 Å.

Bond lengths [Å]		Bond angles [°]	
Pt–C1	2.00	Pt-C1-N1	179
Pt–C2	2.00	C1-Pt-C1	89
Pt–Tl	2.628(3)	C1-Pt-C1′	163
C1–N1	1.15	N1-Tl-N1	81
N1–Tl	2.50	N1-Tl-N1′	132
C2–N2	1.14	Tl-N1-C1	149
N2–Tl	2.29		

Table 3. Crystal structure of $TlPt(CN)_5$ in space group *P*4/*nmm* with Pt and Tl atomic positional parameters from XRD, and C and N parameters derived from the EXAFS results with estimated standard deviations 0.001.

Atom	Site	*x*/*a*	*y*/*a*	*z*/*c*
Pt	2c	1/4	1/4	0.1982(2)
Tl	2c	1/4	1/4	0.8724(2)
C1	8j	0.067	0.067	0.235
C2	2c	1/4	1/4	0.447
N1	8j	–0.0385	–0.0385	0.253
N2	2c	1/4	1/4	0.588

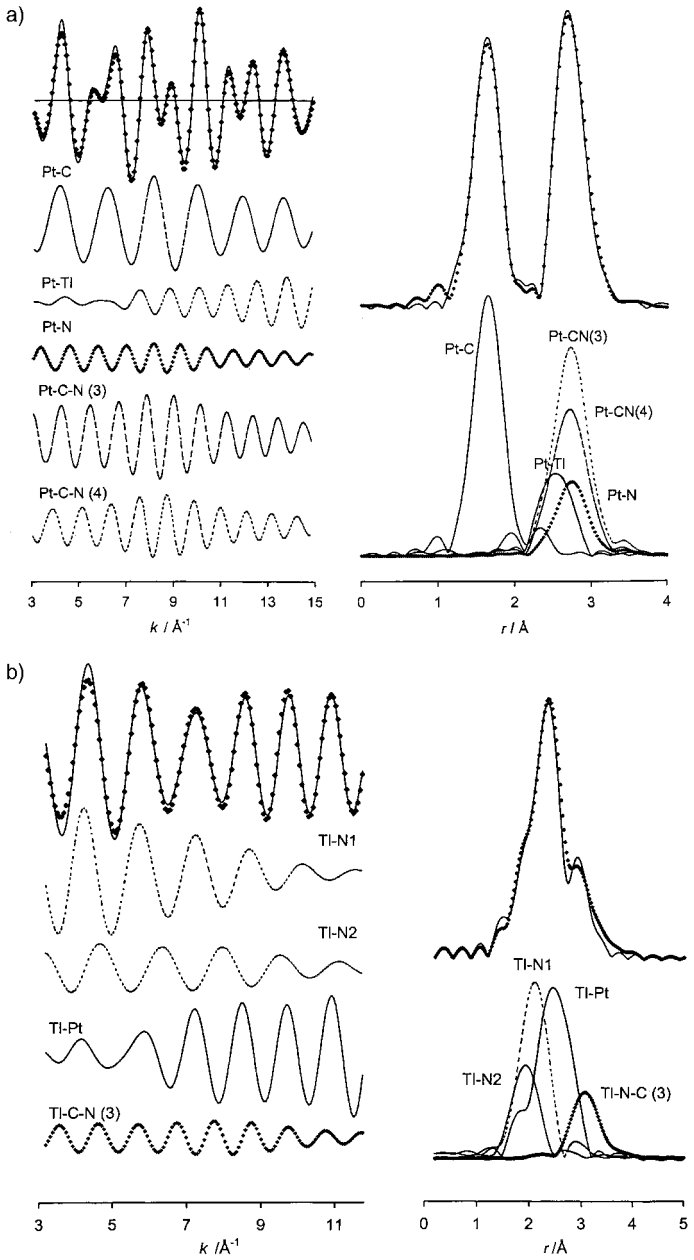

Figure 3. a) Pt L_{III} edge EXAFS of the compound $TlPt(CN)_5$. Left: Filtered k^3-weighted EXAFS function (——) with model fit (◆) (top), and contributions from individual scattering paths. Right: the corresponding Fourier transformations. b) Tl L_{III} edge EXAFS. Left: Filtered k^3-weighted EXAFS function (——) with model fit (◆) (top), and contributions from individual scattering paths. *R*ight: the corresponding Fourier transformations.

The coordination environment of the platinum atom consists of five carbons from the cyano ligands and a thallium atom. It is not possible to discern a significant difference in the Pt–C bond lengths of the axial and equatorial cyano ligands from the XRD or the EXAFS data. The Pt···N distance is 1.14 (axial) and 1.15 Å (equatorial) longer than the Pt–C bond (Table 2); this indicates that the Pt–C–N coordination is close to linear in both cases.[8]

Five nitrogen atoms from the bridging cyano groups surround the thallium atom in a highly distorted octahedral geometry (Figure 2 top). The two Tl–N bond lengths for the cyano groups in the equatorial and axial positions differ significantly and could be refined independently to 2.50(1) and 2.31(3) Å respectively.

Correlation of Pt–Tl bond lengths: The Pt–Tl bond length in the $[(NC)_5Pt–Tl(CN)_n]^{n-}$ ($n=1-3$) species in solution increases from 2.598 to 2.638 Å with an increasing number of the coordinated cyano ligands, n.[6c] Extrapolation of this correlation to $n=0$ would give a Pt–Tl separation of about 2.58 Å for the hydrated $[(NC)_5Pt–Tl(H_2O)_x]$ complex in solution. However, the Pt–Tl bond length in the solid $TlPt(CN)_5$ compound is 2.628 Å. The longer Pt–Tl bond in the solid compound is probably due to the presence of cyanide bridges within and between the antiparallel –N2-C2-Pt-Tl-N2-C2-Pt-Tl– chains. Attraction between the thallium atom and the nitrogen atoms of the strongly bonded linear N2-C2-Pt entities within a chain and between adjacent chains (N1-C1-Pt) (Figure 2 top) can be expected to cause an elongation of the Pt–Tl bond. Recently, Pt–Tl bond lengths were calculated for the $[Tl_2Pt(CN)_4]$ molecule of D_{4h} symmetry.[9] In contrast to the Pt–Tl bond length of 3.14 Å in the crystal structure of this compound,[7b] the bond length in the free molecule is calculated to be 2.877 Å. The much longer Pt–Tl bond length in the crystal was attributed to the electrostatic attraction of the positive thallium ion by the five surrounding negatively charged nitrogen atoms.

Moreover, the Pt-C1-N1-Tl bridges between neighbouring chains hold the cyano ligands in eclipsed positions. Strong π–π repulsion between these antiparallel C1–N1 groups is expected due to the short Pt–Tl bond. This repulsion is assumed to increase the contact distance to about 3.9 Å between the perfectly eclipsed cyano ligands to model the highly symmetrical structure in the space group $D^7_{4h}(P4/nmm)$(Figure 2 top). In this configuration the platinum atom must be slightly displaced from the equatorial plane, which is formed by the carbon atoms, despite four strong Pt–C1 bonds; this gives rise to estimated angles for Tl–N1–C1 of about 149° and for C–Pt–C′ of 163°.

Crystal structures that contain platinum–thallium bonds can be divided into three groups that depend on the formal oxidation states of the metal ions: Pt^0–Tl^I (2.860–3.047 Å),[10] Pt^{II}–Tl^I (2.876–3.152 Å)[7b, 11] and Pt^{II}–Tl^{II} (2.698–2.708 Å)[12]. The $TlPt(CN)_5$ compound has a higher total oxidation state (v) of the two metal atoms than in the solid compounds listed above; this is consistent with the shorter Pt–Tl bond length of 2.628 Å.

Vibrational spectra and force constants: (see Appendix I) The Raman and IR spectra of the compound are shown in Figure 4 and their assignments are based on normal coordinate calculations and given in Table 4. Force constants are listed in Table 5. For an isolated $TlPt(CN)_5$ molecular entity in C_{4v} point group symmetry, there are 30 internal modes that belong to the symmetry species $7A_1+A_2+4B_1+2B_2+8E$. The possible splitting of these 30 internal modes is investigated by factor group analysis for two interacting formula units $TlPt(CN)_5$ (Figure 5) in the space group $P4/nmm$ (D^7_{4h}).[13] For a Bravais cell with $Z=2$, 60 internal fundamental

0947-6539/01/0710-2170 $ 17.50+.50/0 *Chem. Eur. J.* **2001**, *7*, No. 10

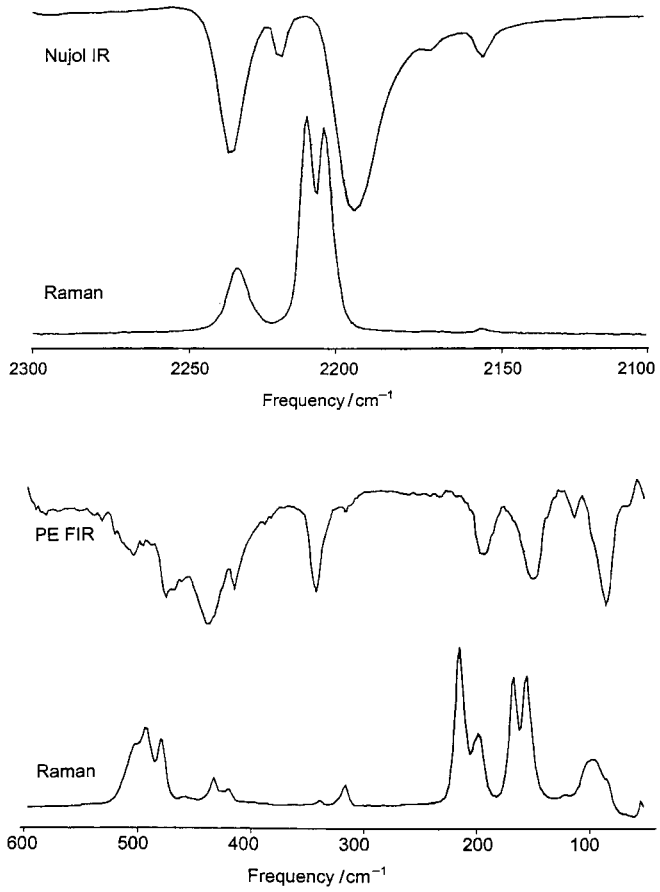

Figure 4. Raman and infrared absorption spectra of the solid compound $TlPt(CN)_5$. Top: Cyanide-stretching region. Bottom: Low-frequency region.

Table 4. Assignment in D_{4h}^7 factor group symmetry of the solid-state infrared absorption (IR) and Raman spectra of the $TlPt(CN)_5$ compound (see Appendix I).

IR [cm^{-1}]	Raman [cm^{-1}]	D_{4h}^7	Description
2235 s		A_{2u}	C–N stretching (axial)
	2233 s	A_{1g}	
2219 w		A_{2u}	C–N stretching (equatorial)
	2210 vs	A_{1g}	
	2205 vs	E_g	
2196 vs		E_u	
2184 w, sh (2186)[a]		(A_{2u})	^{13}C–N stretching (axial)
2170 w (2167)		(E_u)	C^{15}–N stretching (equatorial)
2154 w (2153)		(E_u)	^{13}C–N stretching (equatorial)
	2153 w	B_{1g}	
503 w		A_{2u}	Pt–C stretching (axial)
	501 w	A_{1g}	
	489 m, 476 m	E_g	Pt–CN linear bending (axial)
474 w		E_u	
	456 w	E_g	Pt–C stretching (equatorial)
438 w		E_u	
	431 w	B_{1g}	
	419 w	A_{1g}	
411 vw		A_{2u}	
	398 vw	E_g, B_{1g}	Pt–CN linear bending (equatorial)
343 w		A_{2u}, E_u	
	338 w	A_{1g}, B_{2g}	
317 vw		E_u	
	315 w	E_g	
	211 s	A_{1g}	Pt–Tl stretching
	196 m	B_{1g}	
194 w		A_{2u}	
	164 s, 152 m	E_g	
150 m		E_u	

[a] The calculated isotope bands are given in brackets.

vibrational modes are possible that belong to the following symmetry species:

$\Gamma(\text{internal}) = 7A_{1g} + A_{2g} + 4B_{1g} + 2B_{2g} + 8E_g + A_{1u} + 7A_{2u} + 2B_{1u} + 4B_{2u} + 8E_u$.

Of these, 21 are Raman active vibrational frequencies ($7A_{1g} + 4B_{1g} + 2B_{2g} + 8E_g$), and 15 IR are active ($7A_{2u} + 8E_u$). In principle, no coincidences should occur as there is a centre of symmetry in the unit cell, but the amount of correlation splitting between a pair of Raman and IR modes does depend on the strength of the interaction.

CN stretches: The highest frequency band in the CN-stretching region of the Raman spectrum appears at 2233 cm^{-1}. It is well known that in a M-CN-M′ bridge, the ν(C–N) frequency may shift to higher wavenumbers by more than 40 cm^{-1}.[8] Therefore, this high frequency Raman band can be assigned to the symmetric stretching mode A_{1g} of the axial cyano group, which forms a strong bridge in the linear –Pt-Tl-N2-C2-Pt– chain. The Raman band at the next highest frequency, 2210 cm^{-1} (A_{1g}) is assigned to the stretching frequency of the less strongly bridging equatorial cyano ligands of the platinum atom. The asymmetric stretching frequency, E_g, is found at 2205 cm^{-1}, while the lowest frequency band at 2153 cm^{-1} is assigned to the B_{1g} species.

Table 5 shows that the CN stretching force constant for the axial ligand is about 7% larger than for the equatorial ligands at 18.977×10^{-2} and 17.552×10^{-2} N m^{-1}, respectively.

Pt–C stretching modes: The Pt–C stretching bands for cyano compounds are expected in the region from about 410–500 cm^{-1}.[14, 15] If the highest Raman band at 501 cm^{-1} is assigned to the in-phase Pt–C stretching mode (A_{1g}) of an axial cyano ligand and if the set of bands between 456 and 419 cm^{-1} are assigned to the three Pt–C stretching modes ($A_{1g} + B_{1g} + E_g$) of equatorial cyano ligands (Table 4), the normal coordinate calculations result in a reasonable force field (see Appendix I). The difference between the force constants of the Pt–C stretching vibration for axial and equatorial sites is in agreement with corresponding values for the C–N bond: the larger K(C–N) for the axial cyano ligand corresponds to a smaller K(Pt–C) and vice versa for equatorial ligands (Table 5). This result is consistent with back-donation from platinum to the antibonding orbitals of the cyanide ion.

The force constants show that an axial Pt–C bond is substantially weaker (2.082×10^{-2} N m^{-1}) than the equatorial bonds (2.675×10^{-2} N m^{-1}) (Table 5). In an isolated $[(NC)_5Pt–Tl]$ entity, the *trans* influence of the thallium atom would be expected to give the opposite effect. For σ-bonded complexes of transition metals, the presence of a ligand with strong acceptor (or weak donor) ability, as for thallium in this case, would cause strengthening of the Pt–C_{trans} bond.[16]

Table 5. Force constants calculated for the compound $TlPt(CN)_5$.[a]

	Coordinates involved[b]	Force constants	Units[c]
internal stretches			
K(CN), equatorial	E	17.552	a
f(CN,CN) trans	E,E′	−0.193	a
f(CN,CN) cis	E,E	0.257	a
K(CN) axial	A	18.977	a
K(PtC), equatorial	e	2.675	a
f(PtC, PtC) trans	e,e	0.195	a
f(PtC,PtC) cis	e,e	−0.055	a
K(PtC) axial	a	2.082	a
K(PtTl)	m	1.651	a
intermolecular stretches			
k(Tl…N) equatorial	q (in-chain)[d] 0.900	a	
k(CN,CN) equatorial	(cross-chain)[d] 0.037	a	
k((CN,CN) axial	(in-chain)	−0.008	a
k(PtC,PtC) axial	(in-chain)	0.024	a
k(PtC,PtC) equatorial	(cross-chain)	0.022	a
k(PtTl, PtTl)	(in-chain)	0.083	a
k(PtTl, PtTl)	(cross-chain)	0.133	a
bends			
H(PtC2)equatorial	α	(0.33)[e]	b
h(PtC2, PtC2)	$\alpha\,\alpha$	(−0.15)	b
H(TlPtC)	β	(0.34)	b
h(TlPtC, TlPtC)	$\beta\beta$	(−0.08)	b
H(PtC2) equatorial, axial	φ	(0.34)	b
h(PtC2, PtC2)	$\varphi\varphi$	(−0.08)	b
internal linear bending deformations			
H(PtCN)equatorial	ε	0.304	b
h(PtCN, PtCN)trans	$\varepsilon\,\varepsilon$	0.033	b
h(PtCN, PtCN)cis	$\varepsilon\,\varepsilon$	−0.022	b
H(PtCN)equatorial	ε'	0.287	b
h(PtCN, PtCN)trans	$\varepsilon'\,\varepsilon'$	−0.035	b
h(PtCN, PtCN)cis	$\varepsilon'\,\varepsilon'$	0.014	b
H(PtCN)axial	γ	0.511	b
intermolecular linear bending deformations			
h(PtCN, PtCN)	(cross chain)	0.016	b

[a] K-stretching and H-bending diagonal; k-intermolecular stretch–stretch; f-intramolecular stretch-stretch; h-bend–bend interaction terms; h′-intramolecular interaction of axial PtCN linear bends. [b] See Figure 5 and Supporting Information. [c] a: $10^2\,N\,m^{-1}$; b: $10^{-18}\,N\,m$. [d] In-chain: interactions along axial direction; cross-chain: interaction between molecules in neighbouring chains. [e] Constrained values in brackets.

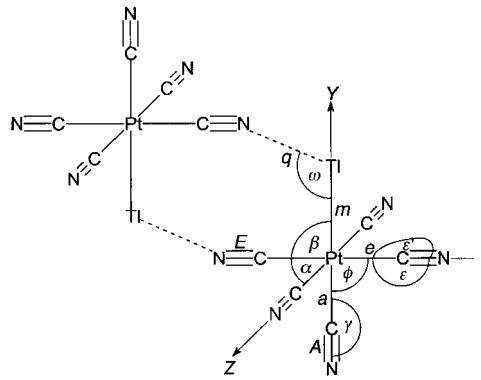

Figure 5. Description of internal coordinates used to calculate the force constants of the unit cell.

Indirect support for this view is given by the NMR results.[6b] The coupling constants $^1J(^{195}Pt,^{13}C)$ for the complex $[(NC)_5Pt{-}Tl(H_2O)_x]$ in solution are substantially larger for the axial Pt–C interaction. However, in the solid compound the $TlPt(CN)_5$ units are connected by two types of CN bridges. In particular the axial (C2–N2) cyano bridge is significantly stronger than the equatorial (C1–N1) bridge, as shown by the Tl–N bond lengths 2.29 Å (axial) and 2.50 Å (equatorial). This results in the reversed order of the Pt–C bond strength.

Pt–Tl stretching modes: The bands which are attributed to metal–metal stretching vibrations usually appear in the low frequency region (250–100 cm^{-1}) of the vibrational spectra.[15, 17] The Raman spectrum of the $TlPt(CN)_5$ compound has four intense bands in two groups in the range 152 and 211 cm^{-1}, and two IR bands at 194 and 150 cm^{-1} (Figure 4). For an isolated $[TlPt(CN)_5]$ complex in C_{4v} point group symmetry a single Pt–Tl stretching band of A_1 symmetry would be expected, which then splits into a pair with one Raman active (A_{1g}) and one IR active (A_{2u}) mode when $Z=2$ in D_{4h}^7 space group symmetry. The number of observed Raman and IR bands shows conclusively that the number of interacting Pt–Tl oscillators must be larger than the two which are present in the crystallographic unit cell. Calculations of frequencies for differently sized segments of the polymeric −N2-C2-Pt-Tl-N2-C2-Pt-Tl− chain showed that there must be strong coupling between neighbouring Pt–Tl stretching oscillators in order to account for the observed large splitting ($\approx$45 cm^{-1}) between the two groups of Raman bands (Table 4). Beside this direct interaction within the chain, there is an additional splitting (15 cm^{-1}) of the Raman bands of the Pt–Tl stretching vibrations; this may be due to a coupling between the chains. This splitting, which is mainly observed in the metal–metal stretching region, is an effect of the large masses of the metal atoms that totally dominate the vibrational coupling. The axial linear bend (Table 4) also splits into a doublet at 489 and 476 cm^{-1}. However, in the C–N stretching region the apparent "doublet" at 2205 and 2210 cm^{-1} can only be assigned to two different types of vibrational modes.

An enlarged Bravais unit cell can be selected to explain the experimental Pt–Tl stretching features; the cell contains eight Pt–Tl pairs within antiparallel neighbouring chains that are connected by bridging equatorial cyano groups. A possible arrangement is shown in Figure 2 (bottom; see also Supporting Information). This set of eight interacting Pt–Tl stretching vibrations can then be assigned to three Raman ($A_{1g}+B_{1g}+E_g$) active species (Table 4) by using the Adam–Newton tables (No. 123, Wyckoff site symmetry 8*s*).[13b] The extra Raman band can be attributed to correlation splitting (which reduces the site symmetry below C_{4v}) of the doubly degenerate E_g mode into the two components at 152 and 164 cm^{-1} (Table 4). The value of the Pt–Tl stretching force constant ($1.651\times10^{-2}\,N\,m^{-1}$, Table 5) is characteristic for single metal–metal bonds.[17b]

An enlarged unit cell is expected to give rise to additional reflections in the powder X-ray diffraction pattern. However, no such extra reflections could be seen. Since these reflections may correspond to alternative positions of only the light C1 and N1 atoms, which may not occur in a regular manner, they may be too weak to be detected.

Electronic characterisation—optical spectroscopy: The presence of a direct Pt–Tl bond is often associated with intense

0947-6539/01/0710-2172 $ 17.50+.50/0 *Chem. Eur. J.* **2001**, *7*, No. 10

photoluminescence, with emission bands in the energy range between 316 and 678 nm.[7b, 11a,c,d, 18] All the compounds reported in these references contain platinum(II) and thallium(I) ions. The white polycrystalline $TlPt(CN)_5$ compound shows a remarkable red luminescence at 700 ± 3 nm when irradiated in the near UV region, and the uncorrected excitation maximum is found at 240 nm. The very large Stokes shift (27730 cm^{-1}) suggests a pronounced structural reorganisation between the ground and excited states. The excitation band correlates well with the absorption spectra obtained from a glycerol suspension of polycrystalline $TlPt(CN)_5$ in which a broad peak is observed at about 270 nm.

The electronic absorption spectrum of the solid $TlPt(CN)_5$ compound is similar to that of an aqueous solution of $[(NC)_5Pt{-}Tl(H_2O)_x]$, which exhibits a broad maximum at 259 nm. The similarity of the monomeric species in solution and the polymeric solid suggests that the optical properties are dominated by the metal–metal interaction and that the cyano bridging either within or between the chains does not have a noticeable effect. Qualitatively, an isolated $[TlPt(CN)_5]$ molecule can be considered to consist of three entities: $[Pt(CN)_4]^{2-}$, CN^- and Tl^{3+}. In C_{4v} point group symmetry, the combination of $5d_{z^2}$ (the HOMO of $[Pt(CN)_4]^{2-}$, which is $5a_{1g}$ and consists of 91% Pt from 76% $5d_{z^2}$ and 15% 6s and 7% CN^- character)[19]),$2p_z$ (the HOMO of CN^-)[8, 20] and 6s (Tl^{3+}) atomic orbitals is symmetry allowed and results in formation of three (bonding, non-bonding and antibonding) three-centre σ molecular orbitals. When the molecular orbitals are filled with two pairs of valence electrons, an antibonding orbital is left empty. We therefore assign the 270 nm absorption to a spin and symmetry allowed $a_{1g} \rightarrow a_{2u}$ ($\sigma^n \rightarrow \sigma^*$) transition.[21]

The experimental results are compatible with this linear three-centre bonding model. Thus, the NMR data of the complex $[(NC)_5Pt{-}Tl(H_2O)_x]$ in aqueous solution reflect the strong interaction between thallium and the axial cyano ligand as indicated by the large (12750 Hz) value of the spin–spin coupling constant $^2J(^{205}Tl,^{13}C)$.[6b] Moreover, a strong spin–spin coupling indicates that the valence s orbitals of thallium participate in the bonding.[22]

X-ray photoelectron spectra (XPS) and charge distribution between the metals: The binding energies of the 4f electrons of the thallium and platinum atoms in the solid compound $TlPt(CN)_5$, 118.2 and 74.9 eV, respectively, were obtained from XPS measurements and can be used to assess the charge distribution of the metal atoms. Binding energies have been determined for thallium and platinum in the compounds with the known oxidation states +1 (Tl_2SO_4, 118.7 eV) and +3 (Tl_2O_3, 117.0 eV), and +2 ($K_2Pt(CN)_4$, 73.0 eV) and +4 ($K_2Pt(CN)_6$, 76.3 eV). If the oxidation numbers of the above compounds are used as reference values, "relative oxidation states" for the Tl and Pt atoms in the bimetallic $TlPt(CN)_5$ compound can be estimated to be 1.6 and 3.2, respectively, from linear interpolation of their corresponding binding energies. A similar charge distribution on the metal atoms in the related complex $[(NC)_5Pt{-}Tl(H_2O)_x]$ in aqueous solution, $Pt^{3.6+}{-}Tl^{1.6+}$, was estimated from the values of ^{195}Pt and ^{205}Tl NMR chemical shifts.[23] The intermediate charges on the metal ions in the compound show that a partial electron transfer has taken place from the platinum to the thallium atom. Hence, if it is considered that the compound is formed in a reaction between platinum(II) and thallium(III) complexes, the Pt–Tl bond can be viewed as a metastable intermediate in the transfer of an electron pair between the metal ions through an inner-sphere mechanism.

Redox decomposition: Thermogravimetric Analysis(TGA) was performed to study the thermal stability of the $TlPt(CN)_5$ compound. Significant decomposition of the sample does not begin until 520 °C. The loss of weight that occurs in a few steps at higher temperature cannot be attributed to stoichiometric decomposition of the compound. On the other hand, when a suspension of the solid compound $TlPt(CN)_5$ is stirred and heated in a slightly alkaline aqueous solution (pH ≈ 8), a homogeneous, transparent and colorless solution is obtained within a few hours at 80 °C. The only thallium species that is observed in the solution by ^{205}Tl NMR was Tl^+, while ^{195}Pt NMR allows the detection of hitherto unknown complexes of Pt^{IV}, namely $[Pt(CN)_5H_2O]^-$ and $[Pt(CN)_5OH]^{2-}$, which exist in pH-controlled equilibrium.[24] The formation of monovalent thallium and tetravalent platinum species with a molar ratio 1:1 and the lack of reaction by-products clearly indicates a redox decomposition of the compound. Thermally induced complementary two-electron transfer between the two coupled metals in the $TlPt(CN)_5$ compound results in cleavage of the metal–metal bond in an irreversible redox reaction. Moreover, the exposure of the compound to an intensive X-ray source (XPS) results in a notable decomposition with formation of tetravalent platinum (see the Experimental Section).

Conclusion

The crystal structure of the compound $TlPt(CN)_5$ has been determined by the combination of XRD and EXAFS results. An unusual network is formed in which three types of bonding is observed between the platinum and thallium atoms. In addition to the direct Pt–Tl bond (2.627 Å), two types of cyano bridges connect the metal atoms. Linear "wires", –NC-Pt-Tl-NC-Pt-Tl–, are formed by linking the $TlPt(CN)_5$ entities through the axial cyano ligand. The bonding within these linear chains is a unique feature of the compound and is substantially stronger than the cyano bridges between the neighbouring chains. While the coordination environment of the platinum atom is the same as in the aqueous solution species $[(NC)_5Pt{-}Tl(H_2O)_x]$, the coordination sphere of the thallium atom in the solid compound contains, besides platinum, five nitrogen atoms from the bridging cyanide groups.

The vibrational spectra show strong coupling between the Pt–Tl stretching vibrations, in particular within the linear chains, but also to the neighbouring antiparallel chains along the *c* axis of the unit cell. Factor group analysis shows that a larger unit cell than the crystallographic unit cell is necessary to explain the results. Thus, a very rare situation is encountered in which the so-called primitive Bravais cell is larger than that required for the crystallographic description.

The compound displays a remarkable red luminescence at 700 ± 3 nm when a glycerol suspension of the polycrystalline sample is irradiated in the near UV region. The corresponding excitation maximum was found at 240 nm and correlates well with the absorption spectrum, which has a broad peak at about 270 nm. The absorption is assigned to a spin and symmetry allowed $a_{1g} \rightarrow a_{2u}$ ($\sigma^n \rightarrow \sigma^*$) transition.

The charge distribution of the metal atoms in the studied compound, which is relative to compounds with known oxidation states and estimated from XPS, is $Pt^{3.2+}$ and $Tl^{1.6+}$. This is close to the previous assessment for the solution species $[(NC)_5Pt{-}Tl(H_2O)_x]$, which was based on the variation of the ^{195}Pt and ^{205}Tl NMR chemical shifts, giving $Pt^{3.6+}$ and $Tl^{1.6+}$. Thus, a substantial electron transfer has taken place from platinum(II) to thallium(III), which is consistent with the strong metal–metal bond.

The complete two-electron transfer corresponds to an irreversible redox reaction. This can be thermally induced and produces monovalent thallium and a pentacyanohydrate complex of tetravalent platinum in the presence of water.

Experimental Section

Materials: The preparation procedures and analytical methods used for the heterobimetallic complexes $[(NC)_5Pt{-}Tl(CN)_n]^{n-}$ ($n = 0-3$) in aqueous solution were fully described in our previous paper.[6b]

Solid $TlPt(CN)_5$ compound: Perchloric acid (3.32 M) was added to an aqueous solution of the dominating complex $[(NC)_5Pt{-}Tl(CN)]^-$ (about 100 mM) until a final free acid concentration of about 1.5 M was reached. Precipitation of the white crystalline powder was promoted by slow evaporation of the solution over silica gel in a vacuum desiccator. The precipitate was filtered, washed with water and 99.5 % ethanol, and dried in vacuum over silica gel for a week until constant weight was achieved. The platinum and thallium content of the solid compound was determined by inductively coupled plasma photometry (ICP) and the carbon and nitrogen content in the solid was determined by elemental analysis (MikroKemi AB, Uppsala, Sweden). Elemental analysis calcd (%) for $TlPtC_5N_5$: Tl 38.7, Pt 36.8, C 11.3, N 13.2; found Tl 39.0, Pt 37.2, C 10.8, N 12.4; Yield: 76%.

NMR measurements: ^{205}Tl NMR spectra of the solutions were recorded with a Bruker AM 400 spectrometer at a probe temperature of 298 ± 0.5 K. Detailed information on typical NMR parameters for recording ^{205}Tl spectra have been given in recent publications from this laboratory.[6b]

Powder X-ray diffraction (XRD): Data collection for the solid $TlPt(CN)_5$ compound was performed with a STOE STADI/P powder diffractometer in symmetric transmission mode, with the crystalline powder in a 0.20 mm glass capillary. Monochromatic $Cu_{K\alpha 1}$ radiation was obtained by means of a germanium monochromator in the incident beam. The sample was rotated to minimise effects of preferred crystal orientation. The total data collection time was 45 h.

The unit cell was determined from accurately measured peak positions in the first part of the diffraction pattern, in which $2\Theta \leq 50^\circ$, by using the program TREOR,[25] and refined with PUDER.[26] The best fit indicators from the refinement of cell parameters were $M_{20} = 21$,[27] and $F_{20} = 27$ (0.0297, 25).[28] The empirical formula, $TlPt(CN)_5$, gives an average atomic volume of 19.6 Å^3 for $Z = 2$.

Two space groups, *P*4/*n* (No. 85) and *P*4/*nmm* (No. 129), were possible from the reflection conditions ($hk0$: $h + k = 2n$ and $0k0$: $k = 2n$) of which *P*4/*nmm* was used for a successful refinement of the structural parameters. The crystal structure was solved manually by combining trial and error technique with difference Fourier maps. The two heavy atoms were located first, followed by the carbon and nitrogen atoms. All Rietveld refinements were performed with a local version of the program DBW 3.2s-8804.[29] The calculation of the positional parameters was made using the SHELXL program (see Supporting Information).[30]

In the Rietveld refinements an empirical absorption correction factor, $\mu_r = 2.2(1)$, was refined[29] and the cell parameters were adjusted to account for nonlinearities of the 2Θ scale. The peak intensities showed negligible preferred orientation effects of the sample, although the peak shapes are somewhat asymmetric and the first peak in the diffraction pattern {001} was clearly much broader, for example, than the third peak {110}. However, the software used did not allow flexible modeling of asymmetry in the peak shapes, and in the first part of the diffraction pattern some discrepancies were seen in the difference between experimental and model powder XRD profiles presented in Figure 1. The peak-shape function used was modified in a pseudo-Voigt manner with an integration range of 20 halfwidths. According to Cagliotti et al.[31] the variation of the halfwidths (in which FWHM = full width half maximum) as a function of Θ is given by Equation (1).

$$\mathrm{FWHM} = U\tan^2\Theta + V\tan\Theta + W \quad (1)$$

The refined parameters U, V and W are given in Table 1. Finally, a zero-point correction, $\Delta\Theta = 0.0954(9)^\circ$, was refined and an asymmetry correction was applied for $2\Theta < 30^\circ$.[32]

The refinement weighting was estimated from counting statistics. All atoms were described with a common isotropic displacement factor, since refinement of individual atomic displacement parameters resulted in very large values for the light atoms without significantly improving the overall fit of the model. The refinement indicated severe serial correlations,[33] which mainly affected the effective standard deviations (esd) of non-structural parameters. The refinement indicators are given in Table 1.

EXAFS:

Data collection: Pt and Tl L_{III} edge EXAFS data were collected in transmission mode by using beamline 4-1 at the Stanford Synchrotron Radiation Laboratory (SSRL). The experimental conditions were similar to those described previously.[34] The energy calibration was made by setting the first inflection point of simultaneously measured platinum or thallium foils to 11564 and 12658 eV, respectively. The usable range of the Pt L_{III} edge EXAFS data is limited to $k < 15$ Å^{-1} by the Tl L_{III} edge, and the Tl L_{III} range to $k < 12$ Å^{-1} by the Pt L_{II} edge at 13273 eV. The sample was diluted with boron nitride (BN) in order to obtain an edge step of approximately one logarithmic unit, and four scans were averaged.

Data treatment: The EXAFSPAK program was used for energy calibration and averaging procedures.[35] The extraction of the EXAFS oscillations, by pre-edge subtraction, data normalisation and spline removal, was performed by means of the WinXAS program.[36] After Fourier transformation (k range 2.6–15 Å^{-1} for the Pt data and 3–12 Å^{-1} for Tl) with a Bessel window function, the k^3-weighted Fourier filtered EXAFS function was fitted to a model function by least-squares refinements of the model parameters. The FEFF 7.0 program was used to evaluate theoretical phase and amplitude functions for single- and multiple-scattering pathways within the assumed molecular entities.[37] The standard deviations, σ, for the refined parameters for the platinum and thallium L_{III} edge data did not include systematic errors (see Supporting Information). However, the variation in the results for different refinement conditions indicated that the accuracy of the distances was within $\pm 3\sigma$.

Models: The Pt L_{III} EXAFS data were dominated by strong multiple scattering from the cyano ligands, which was enhanced by the focusing effect of the nearly linear coordination. The first peak in the Fourier transform corresponded to the Pt–C single-scattering pathway (Figure 3a), but the second peak was much larger than that calculated for a Pt–N single-scattering contribution. This was analysed for the spectra of the standard compounds with the known structures $K_2[Pt^{II}(CN)_4]\cdot 3H_2O$ [7d] (Supporting Information) and $K_2[Pt^{IV}(CN)_6]$ [7e]. Scheme 1 represents the model that was developed to account satisfactorily for both the single- and multiple-scattering contributions from the linear Pt-(C)-N entities and to include three- and four-leg multiple-scattering pathways. The strong multiple scattering obscured the contribution from the Pt–Tl interaction in the Fourier transformation, which must be determined from model fitting of the EXAFS function.

A similar model including multiple scattering (Scheme 1) was also used to describe the contributions to the Tl L_{III} EXAFS from the linearly coordinated Tl–NC entity in the solid $TlPt(CN)_5$ sample (Figure 3b). Fourier filtered EXAFS functions were used for the model fitting to

0947-6539/01/0710-2174 $ 17.50+.50/0 *Chem. Eur. J.* **2001**, *7*, No. 10

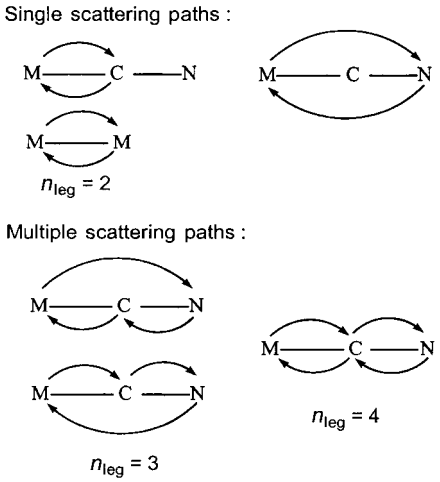

Scheme 1. EXAFS scattering pathways in the linear Pt-C-N units. The degeneracy of the triple scattering path ($n_{leg}=3$) is twice that of the other pathways.

eliminate the contribution from multiple scattering at longer distances in the solid structure (Supporting Information). The most important scattering pathways remaining in the Tl L_{III} Fourier–filtered EXAFS data were found to be Tl–N ($n_{leg}=2$) from the equatorial cyano ligands, and both the Tl–N ($n_{leg}=2$) and Tl–NC ($n_{leg}=3$) scattering paths from the linearly coordinated axial cyano group.

Vibrational spectroscopy: Raman spectra were measured by using a Renishaw Syste 1000 spectrometer, equipped with a Leica DMLM microscope, a 25 mW diode or He–Ne lasers (780 and 633 nm, respectively), and a Peltier cooled CCD detector. Raman spectra were also measured by means of the FT Raman accessory of a Bio–RAD FTS 6000 FT IR spectrometer. The 1024 nm line from a Spectra-Physics Nd-YAG laser was used to irradiate the sample at 150 mW. The mid-infrared absorption spectrum of the solid was measured in Nujol mull, by means of a Perkin–Elmer 1725 FT IR spectrometer. The far-infrared spectra were recorded by means of a Bio–RAD FTS 6000 FT IR spectrometer.

In order to assign the vibrational spectra, factor group analyses were performed, which used both the correlation method[13a] and the Adams–Newton tables [13b]. Wilson's **GF** matrix method was used to calculate the vibrational frequencies by employing a symmetrised valence force field. The initial force constants were adopted from Jones et al.,[14] and refined to give a satisfactory fit to experimental frequencies. The calculations were performed by means of a PC-based program package, written in FORTRAN by J. and L. Mink.[38] For the details of the assignment of the vibrational spectra, see Appendix I.

Absorption and emission spectroscopy: The absorption spectrum of the polycrystalline $TlPt(CN)_5$ compound was recorded as a glycerol suspension in 1 cm cells in a Shimadzu UV–160 spectrophotometer. The emission and excitation spectra of a similar suspension of the compound were recorded with a 1 cm pathlength in a Hitachi F-2000 luminescence spectrometer.

X-ray photoelectron spectroscopy (XPS): For the XPS measurements, powder samples were attached on conductive double-sided sticky tape (fabricate 3M). The nonmonochromatic $Al_{K\alpha}$-excited (15 kV, 15 mA) XPS measurements were performed in the fixed retardation ratio (FRR) mode by a home-made electron spectrometer based on a hemispherical analyser.[39]

The retarding ratio (RR) was ten for the measurements. The relative energy resolution of the analyser related to the pass energy was 0.54 %, and the resolution value was determined experimentally.[40] The vacuum in the measurement chamber was 2×10^{-7} Pa. Survey scans were also measured in FRR mode with the RR = 5.

The binding-energy scale was calibrated to the C 1s line, $E_b=284.6$ eV. In an independent experiment a 1:1 molar ratio mixture of powder samples of $K_2Pt(CN)_6$ and $K_2Pt(CN)_4$ was measured. Only one C 1s line was found to have the same linewidth as that observed for the $TlPt(CN)_5$ sample. This experimental finding indicated that the C 1s photoelectron peak was suitable for energy scale calibration. The C 1s to N 1s binding energy differences were also equal within the experimental error (±0.15 eV) for the mixture of Pt^{II} and Pt^{IV} cyanides and for the $TlPt(CN)_5$ sample; this confirms the reliability of the C 1s line as a reference line.

The XPS spectra were evaluated after the charge correction of the binding energies by means of the EWA computer program.[41] The photoelectron peaks were fitted by a pseudo-Voigt function (Lorentzian–Gaussian sum) after background subtraction. The binding energies for the Pt, Tl, C and N atoms in the compound were determined as: 74.9 (4f, 7/2), 118.2, (4f, 7/2), 284.6 (1s) and 397.6 (1s) eV, respectively.

Some decomposition of the $TlPt(CN)_5$ sample took place after long exposure to X-ray radiation. A new Pt 4f line, which is characteristic for tetravalent platinum, appeared after an hour of irradiation with an intensity which corresponded to 50 % decomposition. A measuring time of less than five minutes was used to avoid the redox reaction; in this case the decay of the compound was negligible.

Thermogravimetric analysis (TGA): The TGA analyses were performed using a recording Mettler TGA/DTA apparatus. Two experiments with 8 mg samples were run at a heating rate of 10 °C min^{-1} in the temperature range 25–1000 °C.

Appendix I

Assignment of the vibrational spectra

CN stretches: Four Raman and three coincident IR bands are expected for the C–N, and also the Pt–C stretching vibrations, of an isolated $Pt(CN)_5$ group with C_{4v} symmetry (in which the symmetry species are $2A_1$, B_1 and E, with only B_1 being Raman active). Since there are two formula units of $TlPt(CN)_5$ that are centrosymmetrically arranged in factor group symmetry D^7_{4h} with site symmetry C_{4v}, these bands will split apart to some extent due to the coupling between the two groups and give noncoincident Raman and IR frequencies. The most intense bands in the cyanide stretching region of the spectra were assigned to these four Raman ($2A_{1g}+B_{1g}+E_g$) and three IR active ($2A_{2u}+E_u$) modes. The observed weak IR bands at 2184, 2170 and 2154 cm^{-1} most likely arise from the natural abundance of the isotopic species $^{13}C^{14}N$ and $^{12}C^{15}N$ (Table 4).

The highest frequency bands in the C–N stretching region at 2233 (Raman) and 2235 cm^{-1} (IR) (Figure 4) can be assigned to the symmetric stretching modes A_{2u} and A_{1g}, respectively, of the bridging axial cyano group in the linear –N2-C2-Pt-Tl-N2-C2-Pt-Tl– chain. The stretching frequency of the bridging equatorial cyano groups forms the next highest pair of frequencies, 2210 (A_{1g}) and 2219 cm^{-1} (A_{2u}), and the asymmetric stretchings E_g (Raman) and E_u (IR), are found at 2205 and 2195 cm^{-1}, respectively. The Raman active band at the lowest frequency 2153 cm^{-1} is assigned to the B_{1g} species.

Pt–C stretching and deformation modes: The Pt–C stretching bands are predicted to occur between 410 and 500 cm^{-1}.[14, 15] The stretching ν(M–C) frequency is generally expected to shift toward lower wavenumbers for a bridging cyano group.[8, 15] However, if we assign the 431 and 438 cm^{-1} bands in the Raman (A_{1g}) and IR (A_{2u}) spectra, respectively, to the downshifted Pt–C stretching frequencies of the axial cyano ligand, and assign the group of Raman and IR bands at higher frequencies (between 456 and 503 cm^{-1}) to Pt–C stretching modes from the equatorial cyano ligands, the calculated stretching force constants become 1.52×10^{-2} and 3.33×10^{-2} N m^{-1} for Pt–C2 and Pt–C1 bonds, respectively. This would be a consequence of the different vibrational coupling in the solid state rather than in the case of noninteracting complexes. This great difference between the force constants of the two Pt–C bonds would lead to a considerable shortening of the equatorial Pt–C bonds and lengthening of the axial bonds, which does not agree with the results of the structural determination (Table 2). Therefore, we propose an assignment of the highest two IR and Raman bands at 503 and 501 cm^{-1} to the out-of-phase and in-phase Pt–C stretching modes of axial cyano ligands, respectively. In addition, when the set of bands between 456 and 411 cm^{-1} is assigned to Pt–C stretches of equatorial cyano ligands, a more realistic force field is obtained for the Pt–C stretching coordinates (Table 5). Consequently, three Raman ($A_{1g}+B_{1g}+E_g$) and two IR ($A_{2u}+E_u$) frequencies in this spectral region are assigned to equatorial Pt–C stretching modes (Table 4).

The bending vibrations of the linear Pt-C-N groups can be assigned to the bands from 489 to 315 cm^{-1},[14] which is in a region that overlaps with the Pt–C stretching modes. The slightly shorter C–N and Pt–C bond lengths of the bridging cyano group relative to those of an equatorial support the assignment of Pt-C-N bends at these relatively high frequencies. For the axial (bridging) cyano group, the Pt–C–N linear bending modes have been assigned to the bands at 489 cm^{-1} Raman (E_g) and 474 cm^{-1} IR (E_u). Five Raman active modes ($A_{1g}+B_{1g}+B_{2g}+2E_g$) and three IR bands ($A_{2u}+2E_u$) are predicted for equatorial Pt-C-N linear bends for two formula units. Due to the small splitting due to weak intramolecular coupling of these modes, we were only able to detect two IR and three Raman bands in this region of the spectra. In Table 4, an assignment is given based on normal-coordinate calculations. However, a band (at 476 cm^{-1}) remains which could not be assigned in the D_{4h}^7 symmetry of the unit cell. This extra band can possibly be interpreted as a consequence of so-called correlation splitting of a degenerate (E) mode from reduced site symmetry.

Pt–Tl stretching modes: A pair of one Raman active (A_{1g}) and one IR active (A_{2u}) Pt–Tl stretching modes is expected for the $TlPt(CN)_5$ complex in C_{4v} point group symmetry for $Z=2$ in the D_{4h}^7 factor group. Instead, four Raman and two noncoincident IR features were observed in the low-frequency region 150–220 cm^{-1}; these correspond to expected stretches of the Pt–Tl metal–metal bond (Figure 4).[15] In order to explain the experimental Pt–Tl stretches, a Bravais cell larger than the crystallographically chosen unit cell must can be used. At least eight Pt–Tl pairs within four antiparallel neighbouring chains, which are connected by the bridging equatorial cyano groups, must be used (Figure 2). Such a set of eight interacting Pt–Tl stretching vibrations can then be assigned to three Raman ($A_{1g}+B_{1g}+E_g$) and two IR ($A_{2u}+E_u$) active species (Table 4), by means of the Adam–Newton tables (No. 123, Wyckoff site symmetry 8*s*).[13b] The extra Raman band can be explained by correlation splitting of the doubly degenerate E_g mode into two components at 152 and 164 cm^{-1} due to site symmetry lower than C_{4v}(Table 4).

These complications require two different model calculations to be performed for a more complete understanding of the solid state spectra. One calculation was carried out for the crystallographic unit cell with two formula units (Figure 5), and the other including eight axial formula units ($Z=8$) (Supporting Information).

The first model explains most of the bands recorded in the solid-state spectra with the exception of the Pt–Tl intermolecular stretches. The six observed Pt–Tl stretching vibrations in the spectra were interpreted by the enlarged cell ($Z=8$) with internal coordinates introduced along the axial directions (Supporting Information).

A number of C–Pt–C and C–Pt–Tl deformational modes with lower intensities are expected below 150 cm^{-1}. The weak Raman bands at 102, 92 and 81 cm^{-1} and the IR bands at 113 and 85 cm^{-1} may result from these modes. Lattice modes are expected to occur below 70 cm^{-1}, since there are heavy atoms involved. The Raman band at 51 cm^{-1} (Figure 4) can be reasonably assigned to the E_g species from the possible rotatory modes ($A_{2g}+E_g+A_{1u}+E_u$). The far-IR spectrum was not measured below 60 cm^{-1}.

The calculated intermolecular interaction force constants are also summarized in Table 5. The strongest in-chain (along the axial direction) and cross-chain couplings (between molecules in neighbouring chains) are those of the Pt–Tl stretchings at 0.083×10^{-2} and 0.133×10^{-2} $N\,m^{-1}$, respectively. We do not have reliable experimental evidence for an intermolecular Tl–N stretching mode. Assuming a force constant of 0.9×10^{-2} $N\,m^{-1}$, the calculated frequencies become 72 and 38 cm^{-1} for the strongly split out-of-phase and in-phase vibrations, respectively. In the extended Bravais cell ($Z=8$), a force constant evaluation suggests that in this second model only the intermolecular cross-chain interaction force constant shows a noticeable change.

Acknowledgement

The continuous financial support of the Swedish Natural Science Research Council (NFR) is gratefully acknowledged. The authors thank the European Commission INTAS Programme, Russian Foundation for Fundamental Research (RFFI 98-03-32651), Carl Trygger Foundation for Scientific Research, Wenner-Gren Center Foundation and the Hungarian National Scientific Research Foundation (OTKA T026115 and T025278) for financial support. We thank the Stanford Synchrotron Radiation Laboratory (SSRL) for allocation of beam-time and laboratory facilities. SSRL is operated by the Department of Energy, Office of Basic Energy Sciences. The SSRL Biotechnology Program is supported by the National Institutes of Health, National Center for Research Resources, Biomedical Technology Program, and by the Department of Energy, Office of Biological and Environmental Research. The authors gratefully acknowledge Prof. Jeffrey K. Nagle (Department of Chemistry, Bowdoin College, Brunswick, USA) for preliminary spectroscopic measurements of the compound.

[1] Y. Wu, B. W. Pfennig, S. L. Sharp, D. R. Ludwig, C. J. Warren, E. P. Vicenzi, A. B. Bocarsly, *Coord. Chem. Rev.* **1997**, *159*, 245–255.
[2] a) B. W. Pfennig, J. V. Lockard, J. L. Cohen, D. F. Watson, D. M. Ho, A. B. Bocarsly, *Inorg. Chem.* **1999**, *38*, 2941–2946; b) G. N. Richardson, U. Brand, H. Vahrenkamp, *Inorg. Chem.* **1999**, *38*, 3070–3079; c) P. V. Bernhardt, B. P. Macpherson, M. Martinez, *Inorg. Chem.* **2000**, *39*, 5203–5208.
[3] C. Chang, D. Ludwig, A. Bocarsly, *Inorg. Chem.* **1998**, *37*, 5467–5473.
[4] H. Vahrenkamp, A. Geib, G. N. Richardson, *J. Chem. Soc. Dalton. Trans.* **1997**, 3643–3651.
[5] A. Vogler, H. Kunkely in *Photosensitization and Photocatalysis Using Inorganic and Organometallic Compounds, Vol. 14* (Eds.: K. Kalyanasundaram, M. Grätzel), Kluwer Academic, Dordrecht, **1993**, pp. 71–111.
[6] a) K. E. Berg, J. Glaser, M. C. Read, I. Tóth, *J. Am. Chem. Soc.* **1995**, *117*, 7550–7551; b) M. Maliarik, K. E. Berg, J. Glaser, M. Sandström, I. Tóth, *Inorg. Chem.* **1998**, *37*, 2910–2919; c) F. Jalilehvand, J. Glaser, M. Maliarik, J. Mink, I. Persson, P. Persson, M. Sandström, I. Tóth, unpublished results; d) M. Maliarik, J. Glaser, I. Tóth, M. W. da Silva, L. Zékány, *Eur. J. Inorg. Chem.* **1998**, 565–570.
[7] a) T. R. Koch, P. L. Johnson, J. M. Williams, *Inorg. Chem.* **1977**, *16*, 640–645; b) J. K. Nagle, A. L. Balch, M. M. Olmstead, *J. Am. Chem. Soc.* **1988**, *110*, 319–321; c) A. I. Yanovskii, K. K. Vaskes, A. V. Babkov, M. Y. Antipin, Y. T. Struchkov, *Koord. Khim.* **1984**, *10*, 1706–1709; d) D. M. Washecheck, S. W. Peterson, A. H. Reis, J. M. Williams, *Inorg. Chem.* **1976**, *15*, 74–78; e) J. Weiss, *Z. Naturforsch. Teil B* **1974**, *29*, 119–120.
[8] A. M. Golub, H. Köller, V. V. Skopenko, *Chemistry of Pseudohalides*, Elsevier, Amsterdam, **1986**.
[9] M. Dolg, P. Pyykkö, N. Runeberg, *Inorg. Chem.* **1996**, *35*, 7450–7451.
[10] a) O. J. Ezomo, M. P. Mingos, I. D. Williams, *J. Chem. Soc. Chem. Comm.* **1987**, 924–925; b) L. Hao, J. J. Vittal, R. J. Puddephatt, *Inorg. Chem.* **1996**, *35*, 269–270; c) V. J. Catalano, B. L. Bennett, R. L. Yson, B. C. Noll, *J. Am. Chem. Soc.* **2000**, *122*, 10056–10062.
[11] a) A. Balch, S. P. Rowley, *J. Am. Chem. Soc.* **1990**, *112*, 6139–6140; b) O. Renn, B. Lippert, *Inorg. Chim. Acta* **1993**, *208*, 219–223; c) R. Uson, J. Fornies, M. Tomas, R. Garde, R. I. Merino, *Inorg. Chem.* **1997**, *36*, 1383–1387; d) I. Ara, J. R. Berenguer, J. Fornies, J. Gomez, E. Lalinde, R. I. Merino, *Inorg. Chem.* **1997**, *36*, 6461–6464; e) W. Bronger, B. Bonsmann, *Z. Anorg. Allg. Chem.* **1995**, *621*, 2083–2088; f) K. O. Klepp, *J. Alloys Compd.* **1993**, *196*, 25–28.
[12] R. Uson, J. Fornies, M. Tomas, R. Garde, P. Alonso, *J. Am. Chem. Soc.* **1995**, *117*, 1837–38.
[13] a) J. R. Ferraro, J. S. Ziomek, *Introductory Group Theory*, 2nd ed., Plenum, New York, **1975**; b) D. Adams, D. C. Newton, *Tables for Factor Group and Point Group Analysis*, BECKMAN RIIC, Croydon (UK), **1970**.
[14] a) M. N. Memering, L. H. Jones, J. C. Bailar, *Inorg. Chem.* **1973**, *12*, 2793–2801; b) L. H. Jones, J. M. Smith, *Inorg. Chem.* **1965**, *4*, 1677–1681; c) L. H. Jones, *Inorganic Vibrational Spectroscopy, Vol. 1*, Marcel Dekker, New York, **1971**; d) G. H. Kubas, L. H. Jones, *Inorg. Chem.* **1974**, *13*, 2816–2819.
[15] K. Nakamoto, *Infrared and Raman Spectra of Inorganic and Coordination Compounds, Part B*, 5th ed., Wiley-Interscience, New York, **1997**.
[16] A. A. Levin, P. N. Dyachkov, *Electronic Structure, Geometry, Isomerism and Transformations in Heteroligand Molecules*, Nauka, Moscow, **1990**.

  0947-6539/01/0710-2176 $ 17.50+.50/0

[17] a) D. F. Shriver, C. B. Cooper in *Advances in Infrared and Raman Spectroscopy*, *Vol. 6* (Eds.: R. J. H. Clark, R. E. Hester) Heyden, London, **1980**, pp. 127–157; b) F. A. Cotton, R. A. Walton, *Multiple Bonds Between Metal Atoms*, 2nd ed., Clarendon, Oxford, **1993**.
[18] a) J. K. Nagle, B. A. Brennan, *J. Am. Chem. Soc.* **1988**, *110*, 5931–5932; b) B. Weissbart, A. L. Balch, D. S. Tinti, *Inorg. Chem.* **1993**, *32*, 2096–2103; c) S. A. Clodfelter, T. M. Doede, B. A. Brennan, J. K. Nagle, D. P. Bender, W. A. Turner, P. M. LaPunzina, *J. Am. Chem. Soc.* **1994**, *116*, 11379–11386.
[19] T. Ziegler, J. K. Nagle, J. G. Snijders, E. J. Baerends, *J. Am. Chem. Soc.* **1989**, *111*, 5631–5635.
[20] A. G. Sharpe in *Comprehensive Coordination Chemistry*, *Vol.* 2, (Eds.: G. Wilkinson, R. D. Gillard, J. A. McCleverty), Pergamon, Oxford, **1987**, pp. 7–14.
[21] A detailed characterisation of the spectroscopic and photophysical properties of the compound is currently under study.
[22] The one bond spin–spin coupling constant $J(^{195}\mathrm{Pt}\text{-}^{205}\mathrm{Tl})$ for the same complex is 71060 Hz.
[23] "Metal–Metal Bond between Transition and Main-Group Metals. Heterobimetallic Platinum-Thallium Cyanide Compounds", M. Maliarik, Tekn. Lic. Thesis, The Royal Institute of Technology, Stockholm, **1999**, p. 53.
[24] M. Maliarik, J. Glaser, I. Tóth, *Inorg. Chem.* **1998**,*37*, 5452–5459.
[25] P.-E. Werner, L. Eriksson, M. Westdahl, *J. Appl. Crystallogr.* **1985**, *18*, 367–370.
[26] L. Eriksson, *Computer program PUDER*, Stockholm University, Structural Chemistry, Stockholm, **1995**.
[27] P. M. de Wolff, *J. Appl. Crystallogr.* **1968**, *1*, 108–113.
[28] G. S. Smith, R. L. Snyder, *J. Appl. Crystallogr.* **1979**, *12*, 60–65.
[29] D. B. Wiles, A. Sakthivel, R. A. Young, *Computer program DBW 3.2S-8804*, School of Physics, Georgia Institute of Technology, Atlanta, **1988**.
[30] G. M. Sheldrick, *Computer Program for the Refinement of Crystal Structures*, University of Göttingen, **1993**.
[31] G. Cagliotti, A. Paoletti, F. P. Ricci, *Nucl. Instrum.* **1958**, *3*, 223—225.
[32] R. J. Hill, H. D. Flack, *J. Appl. Crystallogr.* **1987**, *20*, 356–361.
[33] L. Eriksson, D. Louer, P.-E. Werner, *J. Solid State Chem.* **1989**, *81*, 9.
[34] J. Blixt, J. Glaser, J. Mink, I. Persson, P. Persson, M. Sandström, *J. Am. Chem. Soc.* **1995**, *117*, 5089–5104.
[35] G. N. George, I. J. Pickering, *EXAFSPAK—A Suite of Computer Programs for Analysis of X-Ray Absorption Spectra*, SSRL, Stanford, CA, **1993**.
[36] T. Ressler, *J. Synchrotron Rad.* **1998**, *5*, 118–122.
[37] a) S. I. Zabinsky, J. J. Rehr, A. Ankudinov, R. C. Albers, M. J. Eller, *J. Phys. Rev. B* **1995**, *52*, 2995; b) J. J. Rehr, A. Ankudinov, S. I. Zabinsky, *Catal. Today* **1998**, *39*, 263–269.
[38] J. Mink, L. M. Mink, *Computer Program System for Vibrational Analyses of Polyatomic Molecules.*Available from J. Mink, L. M. Mink, Department of Analytical Chemistry, Veszprém University, P.O. Box 158, H-8201, Veszprém, Hungary.
[39] L. Kövér, D. Varga, I. Cserny, J. Tóth, K. Tõkési, *Surface and Interface Analysis* **1992**, *19*, 9.
[40] J. Tóth, D. Varga, L. Kövér, B. Gruzza, D. Zeze, C. Jardin, G. Gergely, *Vacuum* **1998**, *50*, 473–479.
[41] J. Végh, *EWA: A Spectrum Evaluation Program for XPS/UPS*, Wiley, Montreux, **1995**, pp. 679–683.
[42] J. -F. Berar, P. Lelann, *J. App. Crystallogr.* **1991**, *25*, 1.

Received: September 6, 2000 [F2718]